Intersubband transitions in strained $In_{0.07}Ga_{0.93}As/Al_{0.40}Ga_{0.60}As$ multiple quantum wells and their application to a two-colors photodetector

Danhong Huang and M. O. Manasreh
Phillips Laboratory (PL/VTRP), 3550 Aberdeen Avenue Southeast, Building 426, Kirtland Air Force Base, New Mexico 87117
(Received 30 January 1996; revised manuscript received 11 March 1996)

Infrared absorption spectroscopy is used to study the conduction band intersubband transitions in Si-doped $In_{0.07}Ga_{0.93}As/Al_{0.40}Ga_{0.60}As$ multiple quantum-well structures with the doping being restricted to the well region. The chemical potential determined by the electron density is designed to be above the second subband edge for samples with certain well widths, so that two absorption peaks with a different wavelength would be observed as one of the requirements for a two-colors photodetector. The optical absorption spectra are calculated from which the peak position energies are extracted and compared with the experimental measurements for different well widths. Good agreement between numerical results and experimental data is achieved. In our theory, self-consistent screened Hartree-Fock calculations were performed, which includes the effects of the z-dependent electron effective mass, dielectric constant, and the nonparabolic dispersion. The strain effect is also taken into consideration by the deformation theory. In addition, the calculated optical absorption spectra included the many-body depolarization and excitonlike shifts. [S0163-1829(96)01432-4]

I. INTRODUCTION

There has been increasing interest in multiband infrared detectors for simultaneous imaging in separate wavelength bands.[1–3] One possible design for a two-colors photodetector is a quantum well with at least three confined states to generate large oscillator strengths for all possible intersubband transitions. To achieve this goal, one can increase either the barrier height or well width. In case of doping in the well region, the two-dimensional electron density (n_{2D}) is increased as the well width (L) increases assuming that the three-dimensional doping concentration remains constant. For fixed n_{2D} and barrier material $Al_yGa_{1-y}As$, one can still increase the barrier height by choosing the well material as a ternary alloy $In_xGa_{1-x}As$ instead of GaAs. In a single-particle picture, the electron wave functions and energy subbands are completely decided by the barrier height and well width. When the quantum well is doped with electrons to obtain intersubband transition optical absorption spectra, the Coulomb interaction between electrons becomes very important, which leads to the wave functions and energy levels being dependent on n_{2D} and temperature (T).

One way to monitor the changes in the material optical response is using a weak probe light that induces the intersubband transitions in the materials studied. The optical absorption technique has been proven to be one of the simplest and most applicable methods[4–7] to characterize materials. A full understanding of their optical properties is necessary, because of their potential use as optoelectronic devices such as photodetectors, modulators, and lasers. Early work[8–13] on the intersubband transitions in Si-doped quantum wells showed that the exchange energy has a nontrivial contribution to the subband structure. The design of these photodevices requires an accurate theory for the purpose of device modeling. For the two-colors infrared photodetector, the strength of the two absorption peaks should be comparable, and the separation of the two peaks should be distinguishable. By performing a theoretical modeling including the screened exchange interaction as described in this paper, one can find the optimal condition for the design of the two-colors infrared photodetector.

In this paper, we calculate the optical absorption spectra from which the peak positions are analyzed. In order to compare the theoretical prediction and the experimental measurements, we have included the conduction band shift due to the strain effect, nonparabolic dispersion, screened exchange energy, and depolarization and excitonic shifts. In Ref. 6, the screening to the exchange interaction was neglected, and an infinite-barrier square well model was used to calculate the exchange energy. This will certainly overestimate the exchange energy. In Ref. 13, there are only two bound states in the quantum well. Also, there is no strain effect included, and only the ground state is populated. This excludes the possibility of quantum well as a two-colors photodetector. From the present theoretical analysis, the optical absorption spectra evolving with L is shown. Consequently, the optimal condition for the design of two-colors infrared photodetectors can be obtained. Moreover, the temperature behavior of the observed optical absorption spectra in a 100 Å well width sample is reproduced theoretically and explained as a result of the subband thermal depopulation.

The rest of the paper is organized as follows. In Sec. II, we derive the formula of the self-consistent screened Hartree-Fock calculation. In Sec. III, we generalize the Thomas-Fermi static screening model by including the finite-size electron distribution. In Sec. IV, we obtain the general formula for the linear optical absorption coefficient and refractive index function, which include many-body effects such as collective dipole moment and vertex corrections[14] (excitonlike shift). Experiment, results, and discussions are presented in Sec. V. Finally, we present our conclusions in Sec. VI.

II. SELF-CONSISTENT SCREENED HARTREE-FOCK CALCULATION

When we restrict the selective doping only to the quantum-well region, we can neglect the bending of the conduction band edges in the well and barriers. Therefore, we are able to model an individual $In_xGa_{1-x}As/Al_yGa_{1-y}As$ quantum well by a symmetric and finite square-well potential $V_{QW}(z)=0$ inside the well with a width L and ΔE_c outside the well, where $\Delta E_c=0.57[1.455y+1.53x-0.45x^2]+\delta E_c$ is the barrier height, x and y are the alloy-composition indices for well and barrier materials, respectively, and δE_c is the shift of conduction band edge due to the strain effect. It should be pointed out that the In segregation is not a problem in the present samples, since we have only 7% In in the well materials. Therefore, our assumption of a square well is still valid. The Schrödinger equation, which determines the wave function $\phi_j(z)$ and energy level E_j in the self-consistent Hartree approximation[5,10,13] is

$$\left[-\frac{\hbar^2}{2}\frac{d}{dz}\left(\frac{1}{m^*(z)}\frac{d}{dz}\right)+V_{QW}(z)+V_H(z)\right]\phi_j(z)=E_j\phi_j(z), \tag{1}$$

where $j=1, 2, 3, \ldots$ is the subband index, $m^*(z)$ is m_W, and m_B for well and barrier materials, respectively. By using the virtual-crystal approximation,[5] we find $m_B/m_e=0.0665(1-y)+0.15y$ for the barrier $(Al_yGa_{1-y}As)$ and $m_W/m_e=0.0665(1-x)+0.0225x$ for the well $(In_xGa_{1-x}As)$ materials, where $m_e=9.10956\times10^{-31}$ kg is the free electron mass. The nonparabolic dispersion can be included through[13,15,16]

$$\frac{m_e}{m_W(k)}=1+\frac{E_p}{3}\left[\frac{2}{E_g+\hbar^2k^2/2m_W}+\frac{1}{E_g+\Delta_0+\hbar^2k^2/2m_W}\right], \tag{2}$$

where we have only included the nonparabolic effect for the $In_xGa_{1-x}As$ well material, $m_W(k)$ depends on the wave number k. In Eq. (2), the energy gap, spin-orbit splitting, and interband Kane matrix elements for the $In_xGa_{1-x}As$ layer are[15] $\Delta_0=0.341-0.09x+0.14x^2$ (eV), $E_p=22.71$ (eV), and

$$E_g=1.519-1.53x+0.45x^2-5.405\times10^{-4}\left(\frac{T^2}{204+T}\right)(\text{eV}). \tag{3}$$

Considering that the effective mass of electrons in the well, and barrier materials are different, we obtain an ''average'' effective mass of electrons in the jth subband of the quantum well by using the first-order perturbation theory,[10,13,15]

$$\frac{1}{m_j^*(k)}=\frac{P_j}{m_W(k)}+\frac{1-P_j}{m_B}, \tag{4}$$

where $m_j^*(k)$ depends on both the subband index j and k. In Eq. (4), P_j is the quantum-well dwelling probability, as defined in Ref. 13.

In terms of a deformation theory,[5] we find the shift of the conduction band edge due to the strain effect

$$\delta E_c=2D\epsilon_\parallel\left(\frac{c_{11}-c_{12}}{c_{11}}\right), \tag{5}$$

where $\epsilon_\parallel=(a_B-a_W)/a_W$ is the biaxial strain, $D=-4.55(1-x)-3.6x$ is the deformation potential, $c_{11}=11.88(1-x)+8.33x$ and $c_{12}=5.38(1-x)+4.53x$ are the elastic stiffness constants, and $a_W=5.6533(1-x)+6.0584x$ and $a_B=5.6533(1-y)+5.662y$ are the lattice constants for the well and barrier materials.[16]

In a classical picture, every electron in the quantum well will be acted on by a summarized Coulomb force from all other electrons and ionized donors. The quantum-mechanical counterpart of this force is the Hartree potential in Eq. (1). The Hartree potential is decided from the Poisson's equation[5,10,13]

$$\frac{d}{dz}\left[\epsilon_s(z)\frac{d}{dz}V_H(z)\right]=4\pi e^2[N_{im}(z)-\rho(z)], \tag{6}$$

where $\epsilon_s(z)=4\pi\epsilon_0\epsilon_b(z)$ depending on z, $\epsilon_b(z)$ is the dielectric constant which is taken as $12.04(1-x)+13.43x$ for the well material and $12.04-2.93y$ for the barrier material.[16] The impurity doping profile is $N_{im}(z)=N_{im}^{3D}$ inside the well and zero outside the well, where N_{im}^{3D} denotes the doping concentration. The electron density function in Eq. (6) can be calculated by

$$\rho(z)=2\sum_j|\phi_j(z)|^2\times\left[\frac{1}{2\pi}\int_0^{+\infty}dk\ k\frac{1}{1+\exp\{[E_j(k)-\mu]/k_BT\}}\right], \tag{7}$$

where $E_j(k)$ is the Coulomb renormalized electron kinetic energy, which will be given below. In Eq. (7), μ is the chemical potential. The charge neutrality condition in this system[13] can be used to determine μ self-consistently for a fixed n_{2D}.

The Coulomb interaction will further renormalize the electron kinetic energy calculated from the self-consistent Hartree approximation by adding a screened exchange-interaction effect to it. For the calculated self-consistent Hartree wave functions $\phi_j(z)$ and energy levels E_j, we can include the screened exchange interaction which strongly depends on T and n_{2D}. This allows us to generalize the self-consistent Hartree calculation into the screened self-consistent Hartree-Fock calculations. The renormalized electron kinetic energy used in Eqs. (7) can be calculated through[13,18]

$$E_j(k)=E_j+\frac{\hbar^2k^2}{2m_j^*(k)}+\sum_{i,\mathbf{k}'}n_i(k')\times\left[\sum_n\varepsilon_{in}^{-1}(|\mathbf{k}-\mathbf{k}'|)V_F^{nj}(|\mathbf{k}-\mathbf{k}'|)\right], \tag{8}$$

where $\varepsilon_{in}^{-1}(q_\parallel)$ is the inverse of a generalized Thomas-Fermi static dielectric-function matrix, which will be given below, and the $V_F^{nj}(|\mathbf{k}-\mathbf{k}'|)$ is the exchange-interaction matrix element,[10,13,18]

$$V_F^{nj}(|\mathbf{k}-\mathbf{k}'|) = -\frac{e^2}{2\epsilon_0\epsilon_b|\mathbf{k}-\mathbf{k}'|}\int_{-\infty}^{+\infty}dz\int_{-\infty}^{+\infty}dz'\,\phi_j^*(z) \times\phi_n(z) \times\exp(-|\mathbf{k}-\mathbf{k}'||z-z'|)\phi_n^*(z')\phi_j(z'). \tag{9}$$

As an electron is excited from the nth subband to the jth subband at the z position, there will be another electron simultaneously making an intersubband transition from the jth subband to the nth subband at the z' position. Eventually, there is an exchange between these two indistinguishable electrons at these two positions. Their fermion character contributes a negative sign in the exchange interaction. The Hartree interaction can only produce a shift of the energy level. However, the difference in the energy levels depends weakly only on the subband index, T, and n_{2D}. The exchange interaction also gives rise to an additional nonparabolic dispersion which can shift the peak position and change the line shape.

III. SCREENING OF THE EXCHANGE INTERACTION

The electron-electron interaction can shift μ in the mean-field theory. This gives rise to an induced-charge density in the system, which in turns constrains the electron-electron interaction through the Poisson's equation. From Eq. (7), we can rewrite the electron density function as

$$\rho(z) = \sum_j |\phi_j(z)|^2\mathcal{N}_j(\mu), \tag{10}$$

where

$$\mathcal{N}_j(\mu) = \frac{1}{\pi}\int_0^{+\infty}dk\;kn_j(k). \tag{11}$$

Within the mean-field theory, we treat the electron-electron interaction as an induced potential that is determined through the Poisson's equation,

$$-\nabla^2\psi^{\rm ind}(\mathbf{r}_\parallel,z) = \frac{1}{\epsilon_0\epsilon_b}[\rho^{\rm ext}(\mathbf{r}_\parallel,z)+\rho^{\rm ind}(\mathbf{r}_\parallel,z)], \tag{12}$$

where $\mathbf{r}_\parallel=(x,y)$ is a two-dimensional (2D) position vector in the quantum-well plane, $\epsilon_b=11.9$ is the average background dielectric constant, $\rho^{\rm ext}(\mathbf{r}_\parallel,z)$ is the external test-charge density, and $\rho^{\rm ind}(\mathbf{r}_\parallel,z)$ is the induced-charge density calculated as the additional part of $\rho(z)$, due to the shift of μ by the amount of $-e\psi^{\rm ind}(\mathbf{r}_\parallel,z)$ and is given by[13,17]

$$\rho^{\rm ind}(\mathbf{r}_\parallel,z) = -e^2\psi^{\rm ind}(\mathbf{r}_\parallel,z)\sum_j |\phi_j(z)|^2\frac{d\mathcal{N}_j(\mu)}{d\mu}. \tag{13}$$

Inserting Eq. (13) into Eq. (12), we arrive at

$$-\nabla^2\psi^{\rm ind}(\mathbf{r}_\parallel,z)+2\sum_j |\phi_j(z)|^2q_j^{\rm TF}\overline{\psi_j^{\rm ind}}(\mathbf{r}_\parallel) = \frac{1}{\epsilon_0\epsilon_b}\rho^{\rm ext}(\mathbf{r}_\parallel,z), \tag{14}$$

where we have defined

$$\overline{\psi_j^{\rm ind}}(\mathbf{r}_\parallel) = \int_{-\infty}^{+\infty}dz|\phi_j(z)|^2\psi^{\rm ind}(\mathbf{r}_\parallel,z), \tag{15}$$

and the inverse of the Thomas-Fermi screening length is defined as

$$q_j^{\rm TF} = \frac{e^2}{8\pi\epsilon_0\epsilon_b k_BT}\int_0^{+\infty}dk\;k\cosh^{-2}\left[\frac{E_j(k)-\mu}{2k_BT}\right]. \tag{16}$$

After the following Fourier transformations

$$\psi^{\rm ind}(\mathbf{r}_\parallel,z) = \int\frac{d^2\mathbf{q}_\parallel}{(2\pi)^2}\int\frac{dq_z}{2\pi}\exp[i(\mathbf{q}_\parallel\cdot\mathbf{r}_\parallel+q_zz)]\psi^{\rm ind}(q_\parallel,q_z), \tag{17}$$

$$\overline{\psi_j^{\rm ind}}(\mathbf{r}_\parallel) = \int\frac{d^2\mathbf{q}_\parallel}{(2\pi)^2}\exp(i\mathbf{q}_\parallel\cdot\mathbf{r}_\parallel)\overline{\psi_j^{\rm ind}}(q_\parallel), \tag{18}$$

$$\rho^{\rm ext}(\mathbf{r}_\parallel,z) = \int\frac{d^2\mathbf{q}_\parallel}{(2\pi)^2}\int\frac{dq_z}{2\pi}\exp[i(\mathbf{q}_\parallel\cdot\mathbf{r}_\parallel+q_zz)]\rho^{\rm ext}(q_\parallel,q_z), \tag{19}$$

$$|\phi_j(z)|^2 = \int\frac{dq_z}{2\pi}\exp(iq_zz)f_j(q_z), \tag{20}$$

Eq. (14) reduces to a simple matrix equation,

$$\sum_j\left[\delta_{n,j}+\frac{q_j^{\rm TF}}{q_\parallel}\mathcal{F}_{nj}(q_\parallel)\right]\overline{\psi_j^{\rm ind}}(q_\parallel) = \psi_n^{\rm ext}(q_\parallel), \tag{21}$$

where $q_\parallel$ is the modulus of a 2D wave vector in the quantum-well plane,

$$\mathcal{F}_{nj}(q_\parallel) = 2q_\parallel\int\frac{dq_z}{2\pi}\frac{f_n(-q_z)f_j(q_z)}{q_\parallel^2+q_z^2} = \int_{-\infty}^{+\infty}dz\int_{-\infty}^{+\infty}dz'|\phi_n(z)|^2 \times\exp(-q_\parallel|z-z'|)|\phi_j(z')|^2, \tag{22}$$

is the form factor due to the finite-size electron distribution,

$$\psi_n^{\rm ext}(q_\parallel) = \frac{1}{\epsilon_0\epsilon_b}\int\frac{dq_z}{2\pi}\frac{f_n(-q_z)\rho^{\rm ext}(q_\parallel,q_z)}{q_\parallel^2+q_z^2} = \frac{1}{2\epsilon_0\epsilon_bq_\parallel}\int_{-\infty}^{+\infty}dz\int_{\infty}^{+\infty}dz'|\phi_n(z)|^2 \times\exp(-q_\parallel|z-z'|)\rho^{\rm ext}(q_\parallel,z'), \tag{23}$$

and

$$\overline{\psi_j^{\rm ind}}(q_\parallel) = \int\frac{dq_z}{2\pi}f_j(-q_z)\psi^{\rm ind}(q_\parallel,q_z). \tag{24}$$

From Eq. (21), we find that the static dielectric-function matrix in the generalized Thomas-Fermi model to be

$$\varepsilon_{nj}(q_\parallel) = \delta_{n,j}+\frac{q_j^{\rm TF}}{q_\parallel}\mathcal{F}_{nj}(q_\parallel), \tag{25}$$

which has been used to screen the exchange interaction in Eq. (8).

IV. LINEAR OPTICAL ABSORPTION COEFFICIENT

When an external z-polarized electromagnetic field is applied, the resulting perturbation in the electron density function will produce an optical response from a normal mode of density fluctuation. In the long wavelength limit, only the vertical intersubband transitions (with the same in-plane momentum for the initial and final states) need to be considered. For a probe field interacting weakly with the electrons in the quantum wells, described by a perturbation $\hat{V}$ to the Hamiltonian induced by the probe field, the absorption coefficient is defined as the ratio of the energy absorbed per unit volume and per unit time to the incident flux[19]

$$\beta_{\rm abs}(\omega)=\frac{\hbar\omega}{n(\omega)\sqrt{\epsilon_b}\epsilon_0 c\mathcal{E}^2_{\rm probe}}W(\omega), \tag{26}$$

where $\mathcal{E}_{\rm probe}$ is the amplitude of the probe field, ω is the frequency of the probe field, $n(\omega)$ is the scaled frequency-dependent refractive index function, and $W(\omega)$ is the probability per unit time for the system to make an intersubband transition from an initial state $|i\rangle$ with the energy E_i to a final state $|f\rangle$ with the energy E_f. The intersubband transition probability can be calculated from the Fermi's golden rule (see Ref. 13 and references therein). A straightforward calculation yields

$$\beta_{\rm abs}(\omega)=\frac{\omega\sqrt{\epsilon_b}}{cn(\omega)}[\rho_{\rm ph}(\omega)+1]{\rm Im}\alpha_L(\omega), \tag{27}$$

where

$$\alpha_L(\omega)=\frac{-e}{\mathcal{E}_{\rm probe}LA}\int d\mathbf{r}_\parallel\int dz\,\delta\rho(\mathbf{r}_\parallel,z,\omega)z, \tag{28}$$

is the Lorentz ratio,[13,20] and $\rho_{\rm ph}(\omega)$ is the photon distribution factor.[13] From the Maxwell's equation for any transverse electromagnetic field,[21] we get

$$\frac{1}{\epsilon_b}\nabla^2\mathcal{E}(\mathbf{r},\omega)+\frac{\omega^2}{c^2}[1+{\rm Re}\alpha_L(\omega)]\mathcal{E}(\mathbf{r},\omega)+i\frac{\omega^2}{c^2}{\rm Im}\alpha_L(\omega)\mathcal{E}(\mathbf{r},\omega)=0, \tag{29}$$

from which we can find the dispersion relation by assuming a plane wave form to $\mathcal{E}(\mathbf{r},\omega)$,

$$\left[\frac{\omega}{c}n(\omega)+\frac{i}{2\sqrt{\epsilon_b}}\beta_{\rm abs}(\omega)\right]^2=\frac{\omega^2}{c^2}[1+{\rm Re}\alpha_L(\omega)+i{\rm Im}\alpha_L(\omega)]. \tag{30}$$

Using Eq. (30), we obtain the refractive index function

$$n(\omega)=\frac{1}{\sqrt{2}}\{1+{\rm Re}\alpha_L(\omega)+\sqrt{[1+{\rm Re}\alpha_L(\omega)]^2+[{\rm Im}\alpha_L(\omega)]^2}\}^{1/2}. \tag{31}$$

The Lorentz ratio in Eq. (28) is calculated as[13,20]

$$\alpha_L(\omega)=-\frac{e}{\pi\epsilon_0\epsilon_b\mathcal{E}_{\rm probe}L}\sum_{j,j'}\int_0^{+\infty}dk\;k\rho_{jj'}(k,\omega)F_{j'j}. \tag{32}$$

For noninteracting electrons, the first-order perturbation part of the density-matrix element in the linear response theory can be obtained from the Liouville's equation,[10,13,20]

$$\rho_{jj'}(k,\omega)=e\mathcal{E}_{\rm probe}F_{jj'}\left[\frac{n_j(k)-n_{j'}(k)}{\hbar\omega-E_{j'}(k)+E_j(k)+i\gamma_{jj'}}\right], \tag{33}$$

where $\gamma_{jj'}=(\gamma_j+\gamma_{j'})/2$ is the dephasing rate in the intersubband transition, and the bare dipole moment for noninteracting electrons is

$$F_{jj'}=F^*_{j'j}=\int_{-\infty}^{+\infty}dz\;\phi^*_j(z)z\phi_{j'}(z). \tag{34}$$

In our numerical calculations, we have made use of the phenomenological formula[5,15] for the homogeneous broadening of jth subband and it is given by

$$\gamma_j({\rm meV})=3.144+0.101\times10^{-11}n_{\rm 2D}(10^{11}{\rm cm}^{-2})+2.55\left[\frac{1}{\exp(\hbar\omega_{\rm ph}/k_BT)-1}\right], \tag{35}$$

which depends on T and $n_{\rm 2D}$. In Eq. (35), γ_j is independent of the subband index j, the optical phonon frequency is $\hbar\omega_{\rm ph}=36.7$ meV. The quadratic term of $n_{\rm 2D}$ (Ref. 5) in γ_j is neglected, since the scattering is only proportional to $n_{\rm 2D}$ in the Born approximation.[17]

When an electron is excited to a high subband, it induces a density fluctuation in the neighboring electrons through the long-range Coulomb force. This will introduce a dynamical screening on the bare Coulomb interaction.

In the quantum statistical theory, by adding the Hartree interaction part to the perturbation part of the Hamiltonian, we obtain the density fluctuation[13]

$$\delta\rho(z;\omega)\equiv\int d\mathbf{r}_\parallel\delta\rho(\mathbf{r}_\parallel,z;\omega)=\sum_{j<j'}\phi^*_{j'}(z)\phi_j(z)e\mathcal{E}_{\rm probe}[F_{jj'}+D_{jj'}(\omega)]\chi^{(1)}_{jj'}(\omega), \tag{36}$$

where $D_{jj'}(\omega)$ is the collective dipole moment as a correction to the bare dipole moment $F_{j'j}$, and $\chi^{(1)}_{jj'}(\omega)$ is the susceptibility of the interacting electrons which will be given below. By solving the Poisson's equation for the Hartree interaction in the self-consistent-field theory,[10,13,20] we get the following linear-matrix equation for $n<n'$ (Ref. 13):

$$\sum_{j<j'} D_{jj'}(\omega)\left[\delta_{n,j}\delta_{n',j'}-\chi^{(1)}_{jj'}(\omega)\int_{-\infty}^{+\infty}dz\int_{-\infty}^{+\infty}dz'\,\phi^*_n(z)\phi_{n'}(z)\left(-\frac{e^2}{2\epsilon_0\epsilon_b}\left|z-z'\right|\right)\phi^*_{j'}(z')\phi_j(z')\right]$$
$$=\sum_{j<j'}\chi^{(1)}_{jj'}(\omega)\int_{-\infty}^{+\infty}dz\int_{-\infty}^{+\infty}dz'\,\phi^*_n(z)\phi_{n'}(z)\left(-\frac{e^2}{2\epsilon_0\epsilon_b}\left|z-z'\right|\right)\phi^*_{j'}(z')\phi_j(z'). \quad (37)$$

We can see from Eq. (37) that the screening effect has been included in the dielectric function which is shown as a coefficient matrix.

In Eq. (36), we have introduced the susceptibility of interacting electrons. It is known that at the same time when one of the electrons is excited to a higher subband, it will create a ''hole'' state in the initial occupied subband. This yields an ''excitonic'' interaction between the excited electron and the ''hole'' state.

In Eq. (36), the susceptibility of interacting electrons is

$$\chi^{(1)}_{jj'}(\omega)=\frac{1}{\pi}\int_0^{+\infty}dk\;k\chi^{(0)}_{jj'}(k,\omega)\Gamma_{jj'}(k,\omega), \quad (38)$$

where $j<j'$, and the susceptibility of noninteracting electrons is

$$\chi^{(0)}_{jj'}(k,\omega)=\frac{n_j(k)-n_{j'}(k)}{\hbar\omega-E_{j'}(k)+E_j(k)+i\gamma_{jj'}}+\frac{n_{j'}(k)-n_j(k)}{\hbar\omega+E_{j'}(k)-E_j(k)+i\gamma_{jj'}}. \quad (39)$$

The vertex part, $\Gamma_{jj'}(k,\omega)$, in Eq. (38) is due to the excitonic interaction[14] and can be calculated by summing over all the ladder diagrams. The result of this summation is the following Bethe-Salpeter's equation[13,20] for $j<j'$,

$$\Gamma_{jj'}(k',\omega)=1+\frac{1}{(2\pi)^2}\int d^2\mathbf{k}\chi^{(0)}_{jj'}(k,\omega)\Gamma_{jj'}(k,\omega)\times\left[\sum_{m\leq m'}\varepsilon^{-1}_{jj',mm'}(|\mathbf{k}'-\mathbf{k}|,0)V_F^{mm'}(|\mathbf{k}'-\mathbf{k}|)\right]. \quad (40)$$

In Eq. (40), the small exciton-coupling effect is neglected. We have also used the inverse of a static dielectric-function matrix in the random-phase approximation in this equation to screen the vertex correction. In the random-phase approximation, the intersubband-type Lindhard's dielectric-function matrix for $j<j'$ and $m\leq m'$ can be written as

$$\varepsilon_{jj',mm'}(q_\parallel,\omega)=\delta_{j,m}\delta_{j',m'}-U_{jj',m'm}(q_\parallel)\left\{\frac{2}{(2\pi)^2}\int d^2\mathbf{k}\times\frac{2[n_m(k)-n_{m'}(|\mathbf{k}+\mathbf{q}_\parallel|)][E_{m'}(|\mathbf{k}+\mathbf{q}_\parallel|)-E_m(k)]}{(\hbar\omega+i\gamma_{jj'})^2-[E_{m'}(|\mathbf{k}+\mathbf{q}_\parallel|)-E_m(k)]^2}\right\}, \quad (41)$$

where the intersubband excitation coupling is

$$U_{jj',m'm}(q_\parallel)=\frac{e^2}{2\epsilon_0\epsilon_b q_\parallel}\int_{-\infty}^{+\infty}dz\int_{-\infty}^{+\infty}dz'\,\phi^*_j(z)\phi_{j'}(z)\times\exp(-q_\parallel|z-z'|)\phi^*_{m'}(z')\phi_m(z'). \quad (42)$$

By combining the effects of the collective dipole moment and vertex correction, Eq. (32) can be generalized to

$$\alpha_L(\omega)=-\frac{e^2}{\pi\epsilon_0\epsilon_b L}\sum_{j<j'}F_{j'j}[F_{jj'}+D_{jj'}(\omega)]\times\int_0^{+\infty}dk\;k\chi^{(0)}_{jj'}(k,\omega)\Gamma_{jj'}(k,\omega). \quad (43)$$

The effect due to the screening and vertex correction tends to shift the peak position up and down, respectively. In addition, the screening will shrink the peak width but the vertex correction will expand it.

V. EXPERIMENT, RESULTS, AND DISCUSSIONS

The multiple quantum-well (MQW) structures used in the present study were grown by the molecular-beam epitaxy technique on semi-insulating GaAs substrates. All samples consist of 50 periods and only the $In_{0.07}Ga_{0.93}As$ well regions were Si-doped $\{[Si]=2.0\times10^{18}\ cm^{-3}\}$. The $Al_{0.4}Ga_{0.6}As$ barrier thickness is 100 Å for all samples. The infrared absorption was recorded at the Brewster's angle of GaAs (73°) from the normal using a BOMEM Fourier-transform interferometer. The spectra were recorded and performed using a continuous flow cryostat and T was controlled within ±0.5 K.

The calculated optical absorption spectra at $T=78$ K are shown in Fig. 1 for different L ranging from 55 Å to 200 Å. It is obvious from this figure that only the E_{12} transition can be seen in samples with L smaller than 100 Å. For $L>100$Å, the second energy subband (first excited state) starts to be populated as L increases. Consequently, a second peak becomes observable which is related to E_{23} transition, as shown in the 115 Å well sample. The strength of these two intersubband transitions becomes comparable for the sample of 125 Å well width. As L increases, the first excited state drops below μ causing a phase blocking for E_{12} transition. This is clearly seen in samples with $L>150$ Å, where the strength of the E_{12} transition is decreased dramatically as compared to that of the E_{23} transition.

The theoretical results shown in Fig. 1 were verified experimentally, as shown in Fig. 2. In this figure, we plotted a few intersubband transitions observed at 78 K in samples with different L. We have observed only one intersubband transition (E_{12}) in samples where μ lies between the ground and first excited states ($L\leq100$ Å). However, as L increases

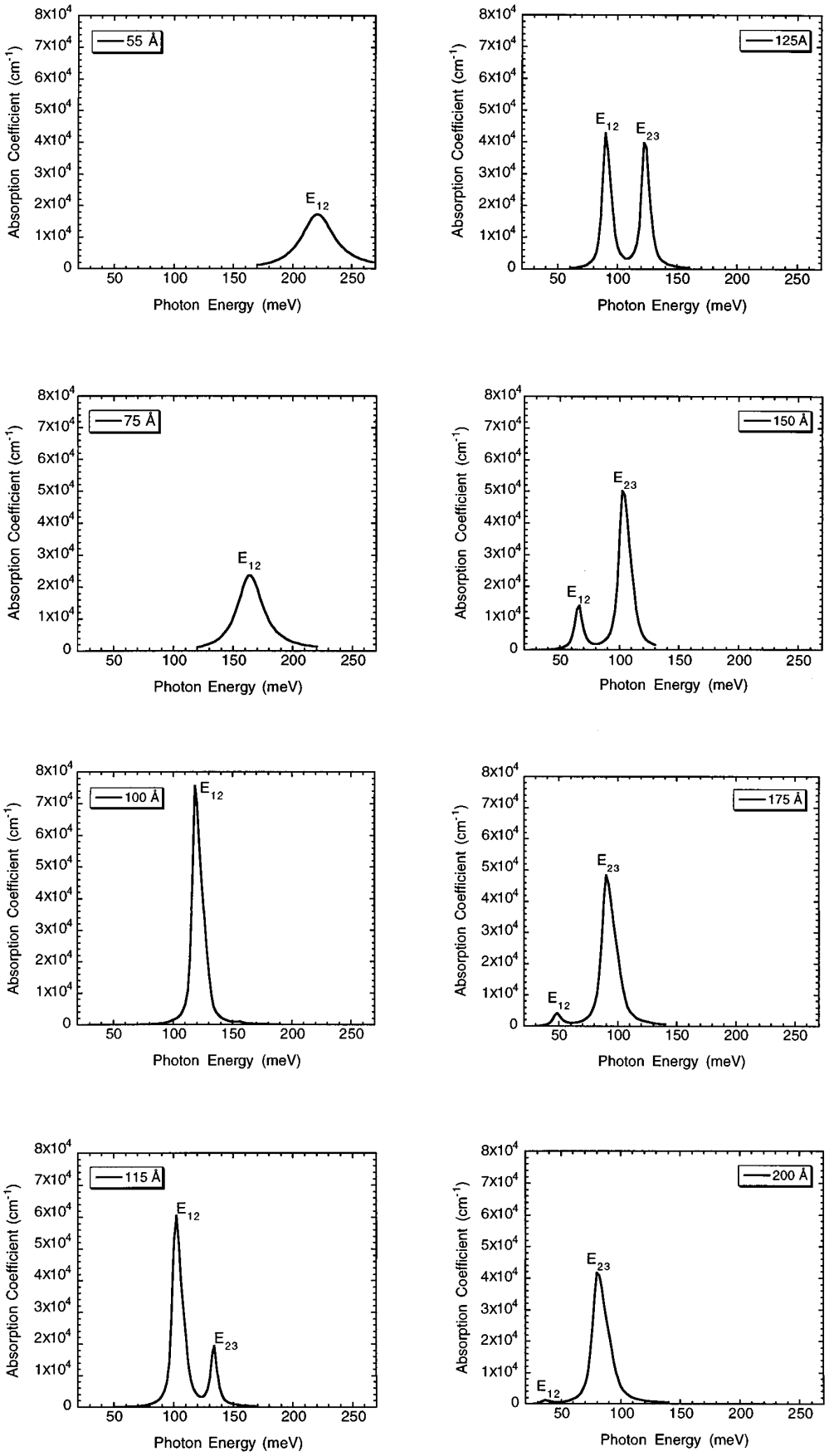

FIG. 1. The calculated evolution of the absorption coefficient spectra for different values of the well width L at $T=78$ K in the $Al_yGa_{1-y}As/In_xGa_{1-x}As$ quantum well with $x=0.07$, $y=0.40$, $n_{\mathrm{im}}^{\mathrm{3D}}=2\times10^{18}$ cm^{-3}. The labels in the figures indicate the well width.

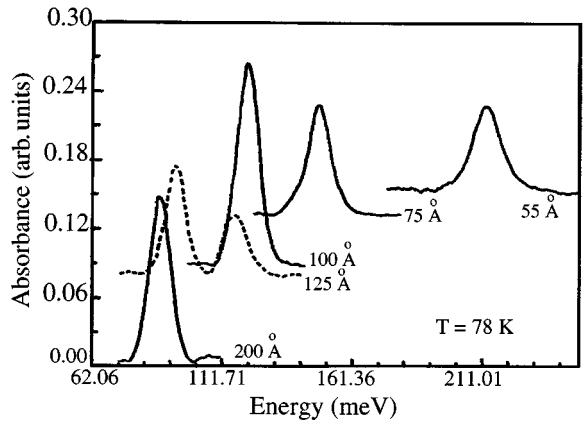

FIG. 2. Optical absorbance as a function of the photon energy for several samples with the well width recorded at $T=78$ K. The sample parameters are the same as those in Fig. 1. The dashed line is for a sample with two intersubband transitions.

above 118 Å we observed two intersubband transitions. As an example, we plotted the spectrum obtained for a 125 Å well sample as the dashed line. For samples with $L>150$ Å, we were unable to observe the E_{12} transition. In addition, the peak position energy of the E_{23} transition becomes almost independent of L for samples with $L>175$ Å.

For direct comparison between theory and experiment, we plotted the peak position energies of E_{12} and E_{23} transitions in Fig. 3 as a function of L. It is clear from this figure that good agreement between theory (solid and dotted lines) and experiment (solid squares and circles) is achieved. It is also noted in Fig. 3 that the separation between two intersubband transitions is increased as L increases. Thus far, we are able to show the following. First, the optical absorption measurements of the intersubband transitions in the $In_{0.07}Ga_{0.93}As/Al_{0.4}Ga_{0.6}As$ MQW show that one transition related to E_{12} is observed in samples in which μ lies between the ground and first excited states. Second, two intersubband transitions related to E_{12} and E_{23} transitions are

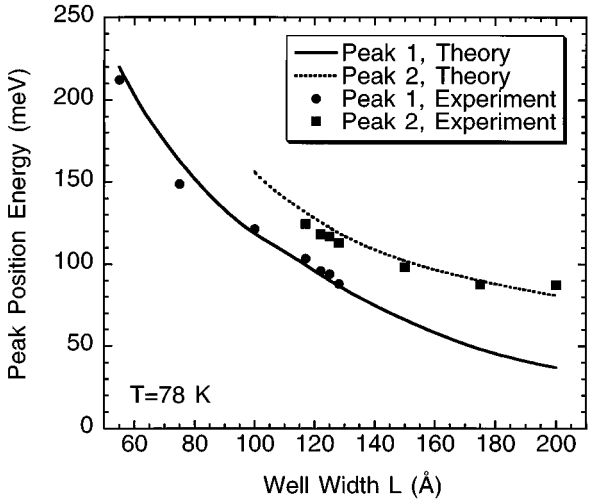

FIG. 3. Comparison of the calculated (lines) and measured (symbols) peaks position energies of the two intersubband transitions related to E_{12} and E_{23} at 78 K, as a function of the well width L.

observed for samples in which μ is above the first excited state. Third, the strength of the E_{12} transition is decreased as μ is raised above the first excited state, which is achieved by increasing L. In fact, we are unable to observe the E_{12} transition in samples with L larger than 175 Å, which can be explained by the phase blocking. The phase blocking is a result of the Pauli's exclusion principle for electrons. Considering that the electrons are excited from the ground state to the first excited state, we know that it can happen only when the initial state is occupied and the final state is empty, or partially empty, at the same time. If μ is above the first excited state, the population in the excited state would block out the electron transition from the ground state to the first excited state. Since the peak strength (intensity) depends strongly on the number of allowed transitions from the ground state to the first excited state, it is then easy to explain the suppression of the E_{12} transition as μ is raised above the first excited state.

It should be pointed out that the line shape of the intersubband transition is not a major subject of this paper. However, the theoretical spectra in Fig. 1 were broadened using Eq. (35) except the first two spectra (samples 55 and 75 Å) which were broadened using a constant. We find this to be necessary in order to compare the experimental and theoretical peak strength E_{12} transition. The broadening issue, however, does not have any implications on the peak position energies.

Additional support to the present theory is based on the temperature behavior of the intersubband transitions in a sample where μ lies very close to the first excited state. In this regard, we recorded the optical absorption spectra of the intersubband transitions in a 100 Å well width sample. The result is shown in Fig. 4(a) in which we presented two spectra observed at 295 and 78 K. From this figure we noted that two intersubband transitions can be clearly seen in the spectrum obtained at 295 K. The large (small) peak is related to the E_{12} (E_{23}) transition. As T is reduced to 78 K, the small peak, which is related to the E_{23} transition, disappeared. This could be easily explained in term of the depopulation of the first excited state as T is decreased. These results were produced theoretically as shown in Fig. 4(b). We plotted in this figure the calculated optical absorption spectra at 78 and 295 K. At $T=78$ K, we find only a E_{12} transition (dashed line) because the first excited state is depopulated. However, at 295 K we can see both E_{12} and E_{23} transitions since the first excited state becomes partially populated at this temperature. The E_{12} transition peak produces a blueshift when T is lowered. This blueshift is due to an exchange interaction effect as it was described earlier.[13] The peak position of E_{23} in our calculation is higher than the one measured in the experiment. Noting that the energy level E_3 is close to the barrier height ΔE_c for $L=100$ Å sample, we expect that the E_3 state can be quite extended in the z direction. Therefore, our infinite barrier model,[5] which puts two infinite barriers 100 Å away from the left and right edges of the quantum well, can overestimate the value of E_3. This is the main reason for the disagreement of E_{23} peak position between the theory and experiment.

The explanation of the temperature behavior observed in the experiment, as shown in Fig. 4(a), can be best understood by showing the depopulation process, as shown in Fig. 5. In

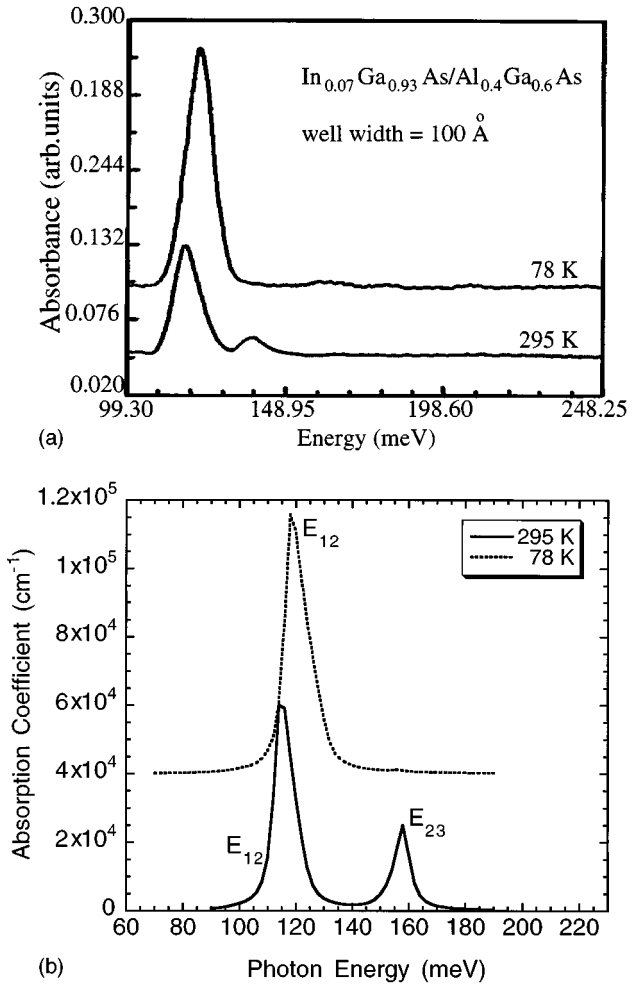

FIG. 4. Comparison between experimental (a) and theoretical (b) spectra taken for a sample with a well width of 100 Å. The two peaks in the spectra measured (calculated) at 295 K are related to the E_{12} and E_{23} transitions and the peak in the spectra measured (calculated) at 78 K is related to the E_{12} transition.

this figure, three energy levels calculated from the self-consistent screened Hartree-Fock approximation, E_1, E_2, and E_3 represented by solid, dashed-dotted, and long-dashed lines, are plotted as a function of L at $T=78$ K. We also plotted μ as the dotted line in this figure. For $L=100$ Å, μ is above the ground state but below the first excited state, which means that the first excited state is depopulated at $T=78$ K. However, when T is raised to 295 K, some electrons will be thermally excited to the first excited state, giving rise to the E_{23} transition, which can be clearly seen in the 295 K spectra in both Figs. 4(a) and 4(b).

VI. CONCLUSIONS

In conclusion, we have established a theoretical model for a two-colors infrared photodetector, which does not contain adjustable parameters. This model was tested against the optical absorption measurements of intersubband transitions in $In_{0.07}Ga_{0.93}As/Al_{0.4}Ga_{0.6}As$ multiple quantum wells. Good agreement between experiment and theory was achieved for the peak position energies of intersubband transitions in samples with different L. The present theoretical model is

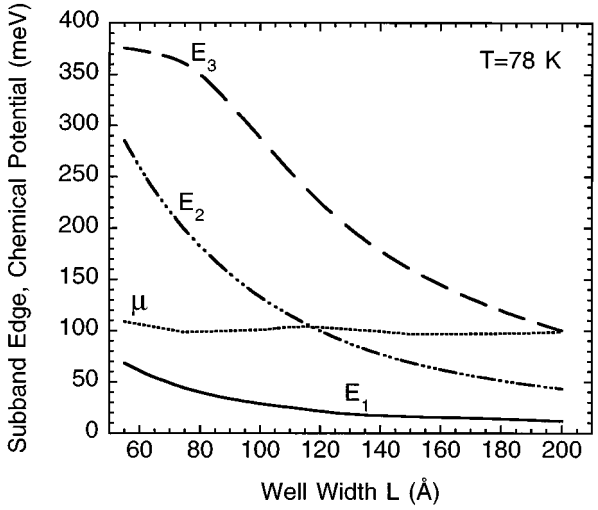

FIG. 5. The calculated energy levels (E_j) and the chemical potential (μ) at $T=78$ K by using the self-consistent screened Hartree-Fock formula as a function of the well width L. The sample parameters are the same as those in Fig. 1. From the bottom to the top, the solid, dashed-dotted, and long-dashed lines represent E_1, E_2, and E_3, respectively. The dotted line corresponds to μ.

based on self-consistent screened Hartree-Fock approximation, which included the effects of the subband- and z-dependent electron effective mass, z-dependent dielectric constant, and the nonparabolic dispersion. The strain effect was incorporated in the current theory using the deformation theory. In addition, the depolarization and excitonlike shifts were included as well.

We have observed experimentally and predicted theoretically that only one intersubband transition exists in the present multiple quantum-well structures in which μ is below the first excited state in the well. As μ is raised above the first excited state by increasing L and keeping the three-dimensional doping constant, we were able to observe and calculate two intersubband transitions. The E_{12} transition, however, suppressed due to phase blocking as μ approaches the second excited state. We also noted that two intersubband transitions related to E_{12} and E_{23} were observed at room temperature for samples in which μ is just below the first excited state. The E_{23} transition was dramatically decreased (disappeared) as T is decreased to 78 K. This observation was explained in terms of thermal depopulation of the first excited state. Finally, we have shown that two intersubband transitions in $In_{0.07}Ga_{0.93}As/Al_{0.4}Ga_{0.6}As$ multiple wells could be observed with equal strength for samples with a well width of 125 Å. These two transitions could be used for two-colors photodetector applications. Future work is focused on the tuning of these two transitions to cover specific wavelength regions, the separation between the two transitions, and the barrier design in which the electrons can be excited and collected under a bias.

ACKNOWLEDGMENTS

One of the authors (D.H.) is supported by the National Research Council.

[1] Kim, S. R. Forrest, M. J. Lange, G. H. Olsen, and M. J. Cohen, IEEE Photon. Technol. Lett. **PFL-6**, 235 (1994).
[2] M. C. Chen and M. J. Bevan, J. Appl. Phys. **78**, 4787 (1995).
[3] Y. Huang and C. Lien, J. Appl. Phys. **77**, 3433 (1995).
[4] M. O. Manasreh, F. Szmulowicz, D. W. Fischer, K. R. Evans, and C. E. Stutz, Appl. Phys. Lett. **57**, 1790 (1990).
[5] M. O. Manasreh and J. P. Loehr, in *Semiconductor Quantum Wells and Superlattices for Long Wavelength Infrared Detectors* (Artech, Boston, 1993), Chap. 2.
[6] M. O. Manasreh, F. Szmulowicz, T. Vaughan, K. R. Evans, C. E. Stutz, and D. W. Fischer, Phys. Rev. B **43**, 9996 (1991).
[7] P. von Allmen *et al.*, Semicond. Sci. Technol. **3**, 1211 (1988); Superlatt. Microstruct. **5**, 259 (1989).
[8] K. Bandara, D. D. Coon, O. Byungsung, Y. F. Lin, and M. H. Francombe, Appl. Phys. Lett. **53**, 1931 (1988).
[9] F. Szmulowicz, M. O. Manasreh, C. E. Stutz, and T. Vaughan, Phys. Rev. B **50**, 11 618 (1994).
[10] G. Gumbs, D. Huang, and J. P. Loehr, Phys. Rev. B **51**, 4321 (1995).
[11] M. Załużny, Solid State Commun. **82**, 565 (1992).
[12] M. Załużny, Phys. Rev. B **43**, 4511 (1991).
[13] D. H. Huang, G. Gumbs, and M. O. Monasreh, Phys. Rev. B **52**, 14 126 (1995).
[14] G. D. Mahan, *Many-Particle Physics* (Plenum, New York, 1981), Chap. 5.
[15] G. Bastard and J. A. Brum, IEEE J. Quantum Electron. **QE- 22**, 1625 (1986).
[16] S. Adachi, J. Appl. Phys. **53**, 8775 (1982); **58**, R1 (1985).
[17] K. Esfarjani, H. R. Glyde, and V. Sa-yakanit, Phys. Rev. B **41**, 1042 (1990).
[18] A. H. MacDonald, J. Phys. C **18**, 1003 (1985).
[19] J. Callaway, *Energy Band Theory* (Academic, New York, 1964), p. 287.
[20] G. Gumbs, D. Huang, Y. Yin, H. Qiang, D. Yan, F. H. Pollak, and T. F. Noble, Phys. Rev. B **48**, 18 328 (1993).
[21] H. Haug and S. W. Koch, *Quantum Theory of the Optical and Electronic Properties of Semiconductors* (World Scientific, Singapore, 1990), p. 12.